Particle-in-cell δf gyrokinetic simulations of the microtearing mode

J. Chowdhury,[1] Yang Chen,[1] Weigang Wan,[1] Scott E. Parker,[1] W. Guttenfelder,[2] and J. M. Canik[3]
[1]*Department of Physics, University of Colorado, Boulder, Colorado 80309, USA*
[2]*Princeton Plasma Physics Laboratory, Princeton, New Jersey 08543, USA*
[3]*Oak Ridge National Laboratory, Oak Ridge, Tennessee 37831, USA*

(Received 24 August 2015; accepted 7 January 2016; published online 26 January 2016)

The linear stability properties of the microtearing mode are investigated in the edge and core regimes of the National Spherical Torus Experiment (NSTX) using the particle-in-cell method based gyrokinetic code GEM. The dependence of the mode on various equilibrium quantities in both regions is compared. While the microtearing mode in the core depends upon the electron-ion collisions, in the edge region, it is found to be weakly dependent on the collisions and exists even when the collision frequency is zero. The electrostatic potential is non-negligible in each of the cases. It plays opposite roles in the core and edge of NSTX. While the microtearing mode is partially stabilized by the electrostatic potential in the core, it has substantial destabilizing effect in the edge. In addition to the spherical tokamak, we also study the microtearing mode for parameters relevant to the core of a standard tokamak. The fundamental characteristics of the mode remain the same; however, the electrostatic potential in this case is destabilizing as opposed to the core of NSTX. The velocity dependence of the collision frequency, which is crucial for the mode to grow in slab calculations, is not required to destabilize the mode in toroidal devices. © *2016 AIP Publishing LLC*. [http://dx.doi.org/10.1063/1.4940333]

I. INTRODUCTION

The microtearing modes are electromagnetic modes with tearing parity which can contribute to the anomalous transport of electrons.[1–11] Unlike the long wavelength tearing mode,[12–14] these microtearing modes are excited by the electron temperature gradient and occur at high n. Recently, a lot of studies report signature of microtearing modes both in the edge[15–17] and in the core[18–25] of spherical tokamaks. Similarly, microtearing modes are reported to be present in the conventional tokamaks[26–32,35,36] as well as in the reverse field pinch.[37,38] These microtearing modes can be precursor to edge localized modes;[35,39] linearly stable subdominant microtearing modes are shown to contribute to the nonlinear electromagnetic ITG turbulence.[40]

The radial perturbation of the magnetic field lines allows the electrons moving along the field lines to traverse also radially. The presence of the electron temperature gradient perpendicular to the magnetic field gives rise to a thermal force proportional to $\hat{b} \cdot \nabla T_e$ ($\hat{b}$ is the unit vector along magnetic field and T_e is the electron temperature) according to the fluid theory. The velocity dependence of the collisions incorporates a time dependence to this force[5] which results in a current perturbation forming a current layer[1–4,6] around the mode rational surface (MRS). In the presence of temperature gradient, the radial motion of the electrons allows the system to relax to lower energy by exchanging heat between hotter and colder regions. It leads to the anomalous transport of heat via the electron channel. The collisions are required "to tap the free energy" stored in ∇T_e.[4] Apart from this time dependent thermal force, in the weakly collisional regime, barely passing electrons in the trapped passing boundary are also shown to produce a current layer[7,8] giving rise to microtearing mode instability.

In the following, we give a qualitative picture of the microtearing mode based on Refs. 2 and 3. We emphasize, however, the fact that this picture is rather simple based on slab geometry which ignores magnetic drifts and trapped particles. Recent comprehensive gyrokinetic analysis has demonstrated the fact that the magnetic drift in the toroidal geometry plays a greater role than the collisions both in the small aspect ratio[17,18] and in the large aspect ratio tokamaks[32] as well as reverse field pinch machine.[37,38] The trapped electrons also play an important role contributing towards the destabilization of the microtearing mode in tokamaks.[17,18,33,34]

The microtearing mode can be found in three regimes of collisionality.[2] The formation of a current layer in these three regimes is determined by the a.c. or d.c. response of the electrons to the perturbation. When one of the conditions $\Omega_{Doppler} = \omega$ or $\tilde{E}_\parallel = 0$ is met away from the MRS, the electrons experience an a.c. field rather than d.c. field, therefore stop the formation of the current layer beyond that point. (Here, $\Omega_{Doppler}$, ω, and $\tilde{E}_\parallel$ are the Doppler shift due to the motion of the electrons along the field line, mode frequency, and parallel electric field, respectively.) Note that $k_\parallel = 0$ at the MRS and therefore, $\Omega_{Doppler}$ is also zero as the latter is a function of $k_\parallel$. Similarly, the electrostatic component of $\tilde{E}_\parallel$, given by $k_\parallel \tilde{\phi}$, is also zero at the MRS. Both $\Omega_{Doppler}$ and $k_\parallel \tilde{\phi}$ develop at finite $k_\parallel$ and become stronger as $k_\parallel$ increases with distance from the MRS. And, at a particular distance from the MRS, either $\Omega_{Doppler}$ becomes equal to ω or $k_\parallel \tilde{\phi}$ component of $\tilde{E}_\parallel$ becomes equal to the inductive component to make $\tilde{E}_\parallel = 0$. Either of these two situations limits the width of the current layer.[2,3]

The collisionless regime[2,3] is defined where the collision frequency is much smaller than the frequency of the mode.

The Doppler frequency $\Omega_{Doppler}$ in this case is $k_\parallel v_\parallel$ as the electrons can freely stream along the magnetic field due to very weak collisions. The width of the current layer $\triangle_\sigma$ is determined by the balance of the mode frequency and the Doppler frequency, that is, $\omega = \Omega_{Doppler}$. This layer is much less than the ion Larmor radius. The width of the electric field layer $\triangle_E$, where the inductive component of $\tilde{E}_\parallel$ is shorted out by the electrostatic component to make $\tilde{E}_\parallel = 0$, is much greater than the current layer. In this circumstance, the electrostatic potential (along with ion dynamics) is assumed to have negligible effect on the microtearing mode.

The second collisionality regime is the semi-collisional regime,[2,3] where the collision frequency is greater than the frequency of the mode. The electron motion, hence, becomes diffusive rather than being free streaming along the field line, so the Doppler frequency becomes $\Omega_{Doppler} = k_\parallel^2 v_\parallel^2/\nu_e$. The current layer is still defined by the balance of the Doppler frequency and the mode frequency because $\Omega_{Doppler} = \omega$ is met before $\tilde{E}_\parallel = 0$ is satisfied. The current layer becomes broader compared to the collisionless case (because one needs to move further away from the MRS to satisfy $\Omega_{Doppler} = \omega$, as $\Omega_{Doppler}$ in the semi-collisional case is less than that in the collisionless case) but is still smaller than the ion Larmor radius.

In the collisional regime, the collision frequency is much higher than the mode frequency.[2,3] The electron motion is highly diffusive, and the Doppler frequency is given by $k_\parallel^2 v_\parallel^2/\nu_e$ which is much smaller than those in the collisionless and semi-collisional cases and also than the mode frequency. Since $\Omega_{Doppler} \ll \omega$, $k_\parallel \tilde{\phi}$ term can rise to a level to short out the inductive component; so, $\tilde{E}_\parallel = 0$ is met before the condition $\Omega_{Doppler} = \omega$ is satisfied. The electrostatic potential $\tilde{\phi}$ then determines the current layer width and plays an important role. The current layer is broadened further compared to the semi-collisional case. The layer width is now bigger than the ion Larmor radius, and the ion dynamics become important.

Analytical theories are available for slab system under various limits to simplify the analysis. The velocity dependence of collisions is required for the mode to be unstable in those limits. These theories are thought to be well representing the microtearing mode even in the toroidal limit as the current layer is expected to be very thin compared to the minor radius. However, neglect of the magnetic drift in these theories is not justified.[2,3] In fact, in a toroidal device, the magnetic drifts can play a crucial role.[17,18] For example, in the core of MAST, the magnetic drift is found to have a significant destabilizing effect, suggesting a resonance between the mode frequency and the magnetic drift frequency.[18] Such a destabilization effect comes mostly through the untrapped electrons. The trapped electrons, another consequence of toroidal geometry, are found to be destabilizing at lower collision frequency and have a stabilizing effect at higher collision frequencies.[18] Similarly, in the edge of MAST, magnetic drifts are found to be strongly destabilizing for the micro-tearing mode.[17] The microtearing modes are found to be stable when magnetic drifts are absent in the edge of MAST. However, the trapped particle drifts are observed to be more important in the edge. Also, the trapped particles are found to provide a direct driving mechanism, and the latter does not require collisions.[17]

Although broad consensus has been observed between theoretical prediction and simulation results of actual experimental parameters, deviations from earlier theories are observed in numerical simulations in certain areas. For example, in the semi-collisional limit, the effect of $\tilde{\phi}$ is neglected and the constant ψ approximation[2] is used. The ion dynamics is also neglected. However, it is later shown that $\tilde{\phi}$ can change the growth rate significantly, and relaxing the constant ψ approximation, indeed, results in reducing the growth of the mode.[3] The ions also can be important even when $\triangle_\sigma < \rho_i$.[41] Moreover, in gyrokinetic simulations of toroidal system, the magnetic drift appears to be playing a crucial role along with electrostatic potential rather than the velocity dependent collisions.[18] The outer region of toroidal geometry is highly populated with trapped electrons which also seem to alter the mode properties significantly.[17]

The role of the electrostatic potential is also found to vary. It is found that $\tilde{\phi}$ is destabilizing or stabilizing depending upon the value of safety factor q;[28,29] $\tilde{\phi}$ has no effect on the linear growth rates of the microtearing mode in the edge of MAST[17] but observed to be strongly destabilizing for the core microtearing mode[18] of MAST. Similarly, the velocity dependence of the collision frequency, which is shown to be essential for the destabilization of microtearing mode in slab geometries, seems to be no longer a strict requirement for the toroidal geometry.[18,25] The magnetic drift is found to be more important in destabilizing the mode in the toroidal geometry than the velocity dependence of the collisions. In fact, when $\tilde{\phi}$ and magnetic drift are set to zero, microtearing mode is found to be completely stable even in the presence of electron temperature gradient, β above threshold, and collisions. However, the role of velocity dependent collisions becomes dominant when the magnetic drift is set to zero in the simulations.[18]

With this background of earlier studies, we carry out a linear study of the microtearing mode in NSTX and standard tokamak using the gyrokinetic code GEM based on the particle-in-cell method.[42,43] With the development of comprehensive gyrokinetic simulations, microtearing mode has been studied in the context of real tokamak plasmas both spherical and conventional. However, to our knowledge, the majority of earlier studies on the microtearing mode in tokamaks are carried out with Eulerian method based gyrokinetic simulations.[15–19,21–25,27,28,30,37] A particle code can provide another verification of the analytical predictions of the earlier theories as well as gyrokinetic simulations using a completely different numerical approach. It is to be noted that GEM has earlier been used to study high n tearing mode in the slab[44] and low n tearing mode in cylindrical geometries.[45,46]

Here, we compare the linear properties of the microtearing mode and its dependence on various equilibrium quantities for two separate shots for which the mode is unstable at the edge and core of NSTX. Although presence of microtearing mode in the edge of NSTX has been reported[15] earlier, a detailed linear analysis is still lacking. The microtearing modes exhibit similar behavior regarding the dependence on β and electron temperature gradient. However, we observe

notable difference in the dependence of the mode on collisions and role of $\tilde{\phi}$ in the instability of microtearing mode in the edge and core. We observe that although the edge of NSTX is highly collisional, the mode growth rate is weakly dependent on the collision frequency and survives even when the collision frequency is zero. Such collision independence of the growth rate is observed in the edge of MAST also[17] and believed to be due to the strong effects of magnetic drifts. We compare the properties of the mode without collisions with that with finite collision frequency for the edge. In contrast to this, the core microtearing mode is found to be strongly dependent on collision frequency and is stable when the collision frequency is zero. We observe contrast in the role of $\tilde{\phi}$ in both cases. While $\tilde{\phi}$ is strongly destabilizing in the edge, it reduces the mode growth rate in the core. In addition to the spherical tokamak parameters, we also simulate a case for conventional tokamak core parameters to compare the microtearing mode properties with those from the spherical tokamak. We have found similar behavior of the mode as far as dependence on β, collisionality, electron temperature gradient, etc., are concerned. However, the effect of $\tilde{\phi}$ appears to be different than what is observed in the core of NSTX. We also tested the effect of velocity dependence of the collision frequency for the case of standard tokamak parameter.

II. THE δf GYROKINETIC SIMULATION MODEL

For the present study, we use the δf, PIC simulation code GEM.[42,43] The main features include electromagnetics with full kinetic electron physics, δf particle-in-cell method, $p_{\|}$ formulation, a split weight scheme for electrons, high β Ampere algorithm, a field line following coordinate system covering $0 < \theta < 2\pi$, and global profile effects. The model includes collisions, equilibrium flow, an arbitrary shaped tokamak equilibrium, and impurity species. Here, we use the local (flux tube) version of GEM.

III. MICROTEARING MODE IN THE EDGE OF NSTX

The parameters for the present study correspond to a discharge in NSTX without lithium coated plasma facing components where the microtearing mode is found to be the dominant instability on the top of the pedestal in the edge. A detailed description of the case can be found in Ref. 15 and references therein. In the following, we present our linear results for the same plasma parameters.

A. Radial variation of microtearing mode

We first perform a radial scan for the real frequency and growth rate of the mode corresponding to $k_\theta \rho_s \approx 1.5$. This is shown in Fig. 1 where the real frequency and growth rate are normalized with respect to the Larmor frequency of Hydrogen ion. The real frequency increases with minor radius r. The growth rate increases with r/a, peaks at around $r/a = 0.93$, decreases, and then finally subsides as r/a is increased further. In Ref. 15, the microtearing mode is found to be the most unstable mode in this region. In the following, we use the parameters corresponding to $r/a = 0.93$. These parameters are as follows: $R/a = 1.364$, elongation $\kappa = 1.642$, triangularity $\delta = 0.384$, safety factor $q_0 = 7.94$, shear $\hat{s} = 7.63$, $T_e/T_i = 1.5$, $T_c/T_i = 1.0$, $\rho_s/a = 0.00705$, $R/L_{Ti} = 4.83$, $R/L_{ne} = 0.9215$, $R/L_{Te} = 7.744, R/L_{nc} = 4.25, R/L_{Tc} = 4.83$, Carbon impurity concentration $n_c/n_e = 0.0356$, electron beta $\beta_e = 0.0169$, $n_e(10^{19}\mathrm{m}^{-3}) = 4.59, Te = 0.207\mathrm{keV}$, $\nu_{ei}(c_s/a) = 5.577$, $Z_{eff} = 1.3$, and no E_r shear. For the linear runs, we consider the following typical numerical parameters: time step $\triangle t c_s/a \approx 8.8 \times 10^{-4}$, for spatial grid size $\triangle x \approx 0.0177\rho_s$, $\triangle y \approx 0.1306\rho_s$, and particle per species $\approx$2 million.

B. Collision scan

We first carry out a collision frequency scan for different values of $k_\theta \rho_s$, namely, 1.08, 1.50, and 1.80 as shown in Fig. 2. Note that the collisions considered here are electron-ion collisions and are modelled as pitch angle scattering. The real frequency increases slowly with collision frequency for all the three values of $k_\theta \rho_s$. The growth rates also change very slowly for all $k_\theta \rho_s$ under consideration. Interestingly, the growth rate of the microtearing mode remains finite even when $\nu_e = 0$. This situation might correspond to the case of collisionless microtearing mode discussed in Ref. 2 where microtearing mode is shown to be independent of collisions when $\nu_e \ll \omega$. But, in the present case, $\omega_r/\nu_e < 1.0$ and $\gamma/\nu_e < 1.0$ (ν_e corresponds to the experimental value in these ratios), and in spite of that, the mode growth rate is independent of collisions. This feature is also at variance with that observed in the semicollisional case studied in Ref. 3 where the growth rate has non-monotonic behavior with respect to the collision frequency. We note that similar behavior of the microtearing mode with respect to the collisions is also observed in the edge of MAST.[17] The presence of a zero collisional branch of the microtearing mode could be due to the fact that in toroidal devices, the magnetic drift

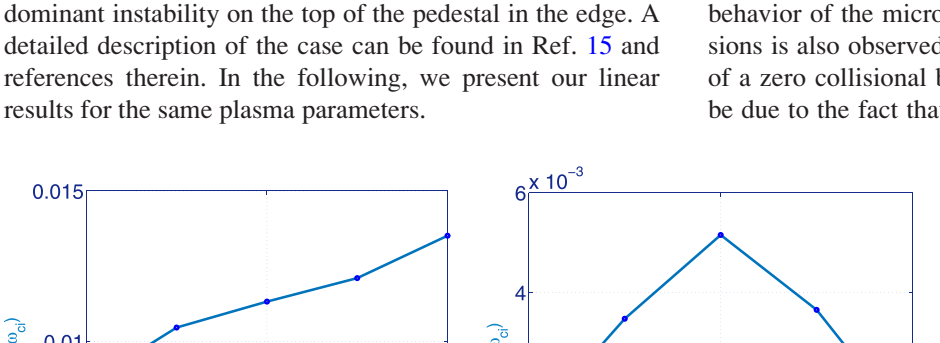

FIG. 1. Real frequency (left) and growth rate (right) vs radial location near edge for $k_\theta \rho_s \approx 1.5$.

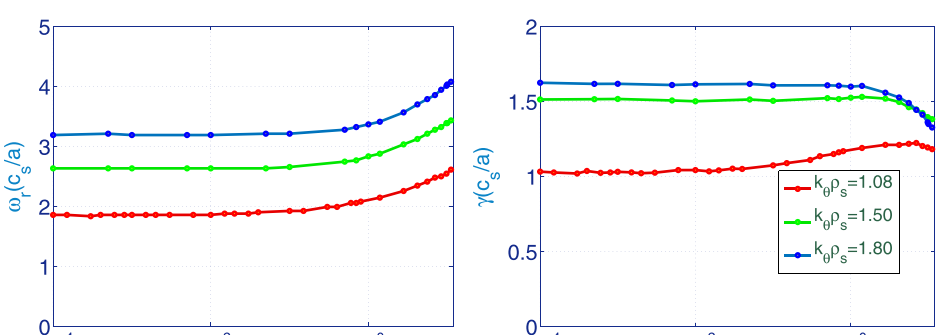

FIG. 2. Real frequency (left) and growth rate (right) vs collision frequency at $r/a = 0.93$ for $k_\theta \rho_s = 1.08, 1.5$, and 1.8.

and trapped particles are more important than the collisions to render the mode unstable.[17,32–34,37,38]

The conditions for the semi-collisional microtearing mode from Ref. 2 are

$$\omega^{*1/3}\gamma_k^{2/3}(\rho_i/\triangle_k)^{4/3} \gg \nu_e \gg \omega^*, \quad \&, \quad \omega^* \gg (\nu_e\gamma_k^2)^{1/3},$$

where $\omega^* = Re(\omega)$. These conditions can be rearranged to give

$$\left[\frac{\omega^*\gamma_k^2}{\nu_e^3}\left(\frac{\rho_i}{\triangle_k}\right)^4\right]^{1/3} \gg 1, \quad \&, \quad \frac{\omega^*}{(\nu_e\gamma_k^2)^{1/3}} \gg 1. \tag{1}$$

Similarly for collisional case, the conditions can be cast into the form[2]

$$\frac{\nu_e}{\omega^{*1/3}\gamma_k^{2/3}(\rho_i/\triangle_k)^{4/3}} \gg 1, \quad \&, \quad \frac{\omega^*}{\gamma_k^{2/5}\nu_e^{3/5}(\triangle_k/\rho_i)^{2/5}} \gg 1. \tag{2}$$

Here, $\gamma_k = \frac{k_y v_e(\triangle' a)}{2\pi^{1/2}k_0^2 a L_s}$, $\triangle_k = \frac{\triangle' a}{2\pi}k_0^2 a$, $\triangle' = \frac{1}{A_\parallel(0)}\frac{dA_\parallel}{dx}\big|_{-\triangle}^{\triangle}$, where $k_0 = \omega_{pe}/c$ is the inverse of skin depth, L_s is the shear length, a is the minor radius, k_y is the wave vector, and v_e is the electron thermal velocity. Also

$$\omega^* = Re(\omega) = \omega_n^* + 5\omega_T^*/4, \tag{3}$$

$$\omega^* = Re(\omega) = \omega_n^* + 5\omega_T^*/2, \tag{4}$$

respectively, are real frequencies for the semi-collisional and collisional cases. Putting the experimental values back in Eqs. (1) and (2) and estimating $\triangle'$ in $\triangle_k$ by using the relation $\triangle' \sim -2k_y$ valid for high n, for $k_\theta\rho_s = 1.5$, we find that the first and second ratios in Eq. (1) turn out to be grater than 1.0. Therefore, the mode theoretically falls in the category of semicollisional regime. The width of the current layer in the semi-collisional case,[2] under the assumption $k_\parallel^2 v_\parallel^2/\nu_e = \omega^*$ where $k_\parallel = k_y\triangle/Ls$, is given by

$$\triangle_\sigma \simeq \triangle_k \frac{(\omega^*\nu_e)^{1/2}}{\gamma_k}. \tag{5}$$

Putting the values as above, for $k_\theta\rho_s = 1.5$, we get $\frac{\triangle_\sigma}{\rho_i} \simeq 0.26$. However, the width of the current layer calculated from the perturbed parallel current as full width at half maximum from our simulation is found to be approximately $0.4\rho_i$ which is larger than the theoretical estimate. But, in either case, $\triangle_\sigma < \rho_i$, as required in the semicollisional case. We would like to add a caveat that although we have compared the properties of the present microtearing mode with those of Drake and Lee,[2] the latter calculations are valid only for slab geometry where the magnetic drifts are missing. Note that the microtearing mode in the present study exhibits an unstable collisionless branch also. The existence of such an unstable microtearing mode at zero collision frequency is suggested to be due to the strong magnetic drifts inherent in spherical tokamaks.[17]

C. Dispersion plot

The relations of the real frequency and growth rate of the mode with $k_\theta\rho_s$ are shown in Fig. 3 for the two cases with $\nu_e = 0$ and $\nu_e = 5.577$. The real frequency ω_r increases almost linearly with $k_\theta\rho_s$. The reason for it is that the real frequency is dependent upon the drift frequencies produced by density and temperature gradients, ω_{*n} and ω_{*T}, which increase linearly with $k_\theta\rho_s$ as shown in Eq. (3). For each value of $k_\theta\rho_s$, the real frequency is higher for $\nu_e = 5.577$ than that

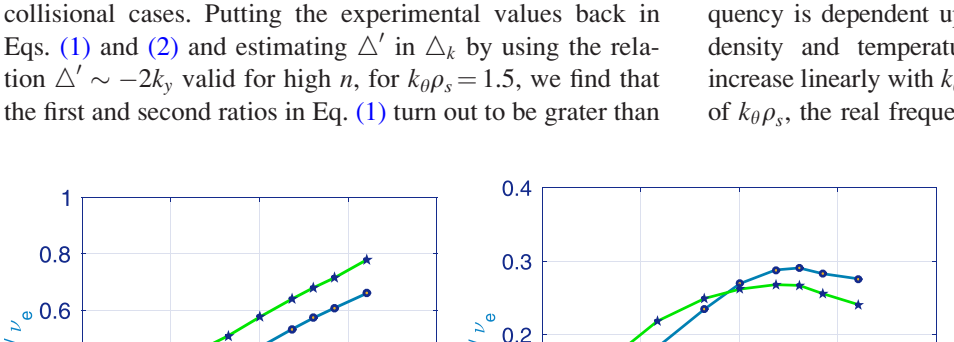

FIG. 3. Real frequency (left) and growth rate (right) vs $k_\theta\rho_s$ at $r/a = 0.93$ for $\nu_e = 0.0$ and $\nu_e = 5.577$.

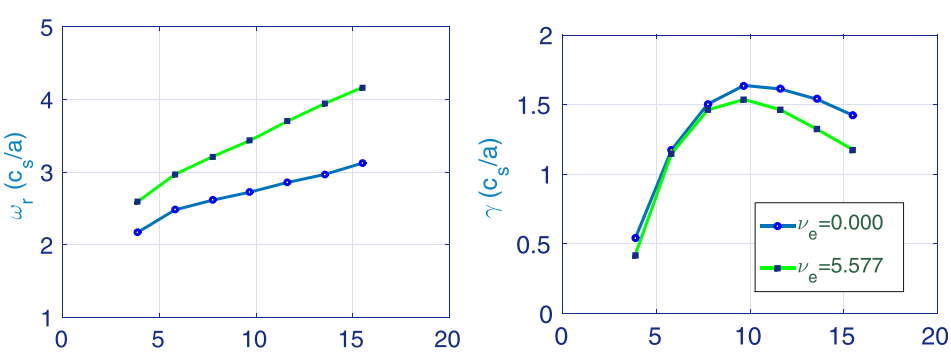

FIG. 4. Real frequency (left) and growth rate (right) vs electron temperature gradient at $r/a = 0.93$ for $\nu_e = 0.0$ and $\nu_e = 5.577$ for $k_\theta \rho_s \simeq 1.5$.

for $\nu_e = 0$. The growth rate increases initially with $k_\theta \rho_s$, peaks around $k_\theta \rho_s \simeq 1.8$, and then starts to roll off. For $k_\theta \rho_s < 1.5$, the growth rates are higher for $\nu_e = 5.577$, but for $k_\theta \rho_s > 1.5$, the $\nu_e = 0$ case exhibits higher growth rates. The microtearing modes, in the simplest case, are the results of two effects,[3] namely, the destabilization by the temperature gradient and stabilization by the magnetic field line bending.[2] Therefore, the growth rate increases with $k_\theta \rho_s$ as the gradient driven terms are dependent on $k_\theta \rho_s$ while decreases at higher $k_\theta \rho_s$ as the magnetic field line bending term becomes dominant, as $\triangle' \sim -k_y \sim -n$ to overcome destabilization by ∇T_e. We do not go much beyond $k_\theta \rho_s = 2$, as the simulation model used here implements 4 point averaging scheme for gyroaveraging, which is accurate for $k_\theta \rho_s \leq 2.0$.[47]

D. Effect of electron temperature gradient

Next, we test for the driving mechanism of the mode. The microtearing modes are unstable only when finite electron temperature gradient is available. Otherwise, $\triangle'$ is negative for higher n or shorter scales and, therefore, "magnetically unfavorable".[2–4] We vary the electron temperature gradient by varying R/L_{Te} for the $\nu_e = 0$, and 5.577 cases. The results are shown in Fig. 4 for $k_\theta \rho_s \simeq 1.5$. The real frequency increases almost linearly with R/L_{Te}. It is expected as the real frequency $\omega \sim \omega_{*,e}$ as shown in Eqs. (3) and (4), [2,3] and, therefore, contingent on R/L_{Te} for given $k_\theta \rho_s$ and R/L_n. The growth rate increases linearly with R/L_{Te} initially, indicating it to be the source of free energy of the mode. However, if we go on increasing the gradient drive, one point is reached where the mode growth rate actually starts decreasing with R/L_{T_e}. In a simple sheared slab model, it is shown that the microtearing mode is the result of competition between the stabilization from magnetic energy and destabilization from the temperature gradient.[2,3,11] It is also shown that the electron temperature gradient also increases the magnetic perturbation of the mode,[3,11] and therefore, it eventually adds to the increase in the magnetic energy. When this combined stabilizing effect becomes stronger than the destabilizing effect, the mode starts decaying. At higher R/L_{Te}, the growth rate is lower for the finite collisional case in comparison with that for the zero collisional case, implying that collisions are slightly stabilizing there. That is because the collisions may further diffuse electrons from the current layer which has already become weaker. This non-monotonic behavior with R/L_{Te} is reported in Ref. 3 in slab geometry, and also in tokamaks,[18,30] and is argued to be the result of including $\tilde{\phi}$ and non-constant ψ across the current layer[3] and complex geometry and trapped electrons in tokamaks.[18]

E. β_e dependence

The effect of β is investigated by varying the electron β_e and calculating the real frequency and growth rate. These are plotted in Fig. 5 for $k_\theta \rho_s \simeq 1.5$. The real frequency is higher for the finite collisional case and decreases with increasing β_e. The growth rate, on the other hand, increases with β_e initially for both cases. This is expected for an electromagnetic mode because β_e can enhance $\tilde{A}_\parallel$ fluctuations through the Ampere equation.[17] At higher β_e, the mode growth rate, however, starts decreasing because of growing stabilizing effect of magnetic energy.[3,11] The mode is stabilized at very low β_e and shows finite growth above a threshold value of β_e. In order to be able to perturb the magnetic field, one requires a certain amount of β;[18] hence, we see a threshold

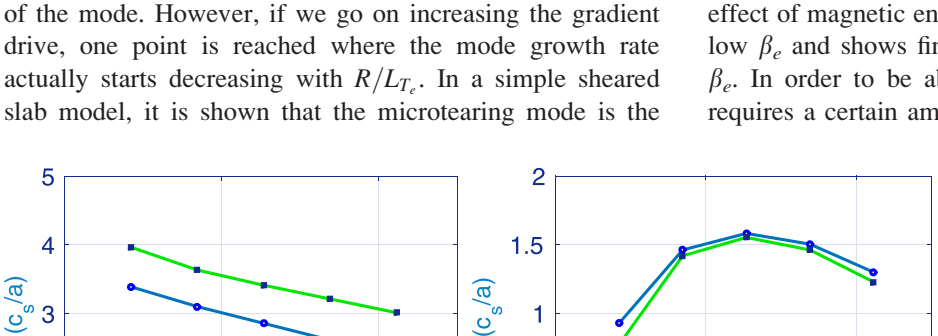

FIG. 5. Real frequency (left) and growth rate (right) vs electron β at $r/a = 0.93$ for $\nu_e = 0.0$ and $\nu_e = 5.577$ for $k_\theta \rho_s \simeq 1.5$.

in β_e. Note that, although β_e is very high in the present case, $\tilde{B}_\parallel$ fluctuations should not have significant effect on the mode.[17,18,23,24] In an alternative way, the stabilization at higher R/L_{Te} and β_e can be seen intuitively as follows: the current perturbations generated by these parameters cannot grow indefinitely, as, at some point, it is reduced either by the balance of the mode frequency and the Doppler frequency ($\Omega_{Doppler} = \omega$ condition) or by attaining the $\tilde{E}_\parallel = 0$ condition, whichever is satisfied first, depending upon the collisionality regime. The electrons see an a.c. field beyond that point.

F. Mode structures of microtearing modes for ν_e=0.0 and ν_e=5.577

The typical mode structures for $\tilde{\phi}$ and $\tilde{A}_\parallel$ are shown in Figs. 6 and 7 for the cases with $\nu_e = 0$ and 5.577. The magnitudes of the potentials are normalized by the maximum value of $A_\parallel$ in each case. There are no conspicuous differences in the mode structures of the mode for $\nu_e = 0$ and 5.577. The electrostatic potential $\tilde{\phi}$ is odd and $\tilde{A}_\parallel$ is even with respect to the ballooning angle θ in both the cases. This is one of the basic characteristics of the microtearing modes which set them distinguished from other electromagnetic modes, for example, KPBM or KBM[48] or other electron electrostatic modes such as ETG/TEM.[56–58] Note that $\tilde{\phi}$ is more extended in θ than $\tilde{A}_\parallel$ because of the fast motion of the electrons parallel to the magnetic field.[19]

G. Effect of density gradient

Scans for real frequency and growth rate by varying electron density gradient are carried out for the mode $k_\theta \rho_s \simeq 1.5$ for finite collisions and are shown in Fig. 8. In doing so, the ion density gradient is also changed to keep the plasma quasineutral, while impurity concentration and density gradient are held constant. The real frequency shown in Fig. 8 changes very weakly with respect to the electron density gradient. The growth rate peaks around $R/L_{ne} \simeq 0.5$ and then decays with increasing density gradient. The mode exhibits

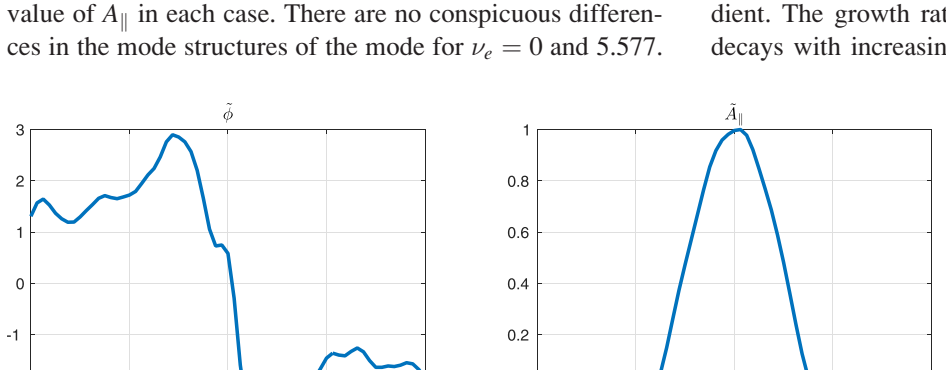

FIG. 6. Mode structures of $\tilde{\phi}$ (left) and $\tilde{A}_\parallel$ (right) for $\nu_e = 0.0$.

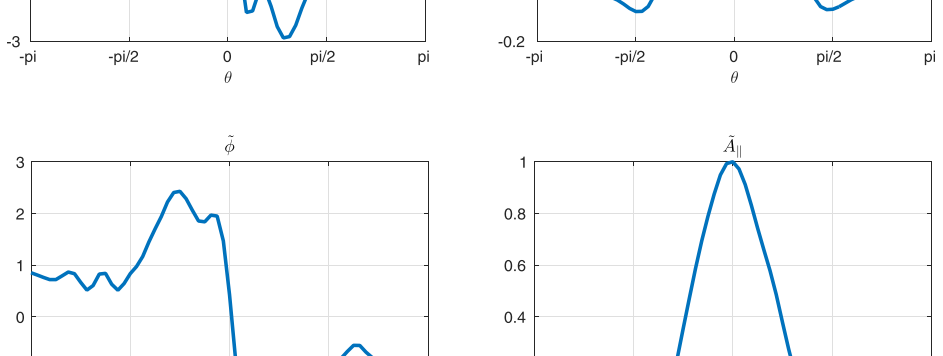

FIG. 7. Mode structures of $\tilde{\phi}$ (left) and $\tilde{A}_\parallel$ (right) for $\nu_e = 5.577$.

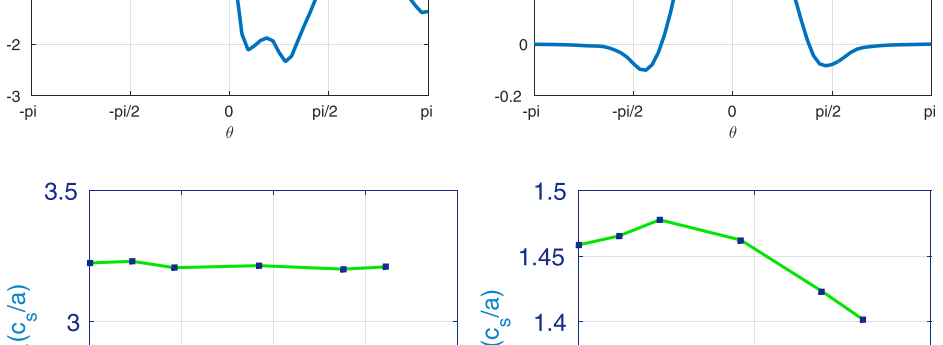

FIG. 8. Real frequency (left) and growth rate (right) vs electron density gradient for $k_\theta \rho_s = 1.5$.

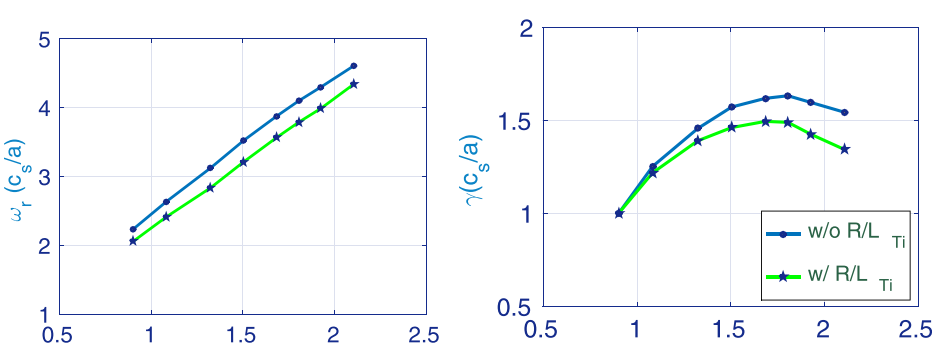

FIG. 9. Real frequency (left) and growth rate (right) vs $k_\theta \rho_s$ at $r/a = 0.93$, with and without ion temperature gradient.

finite growth rate even at $R/L_{ne} \simeq 0.0$. Similar observations are also reported in Ref. 17. The stabilization with increasing R/L_{ne} can be explained as follows: in the presence of density gradient, expansion of plasma also takes place along with convection due to the temperature gradient. When the plasma moves from a hotter to a colder region, it also moves from a denser to a more dilute region simultaneously. So, cooling due to expansion and heating due to convection compete with each other. The expansion of plasma absorbs a certain amount of free energy available to the mode; therefore, the mode growth rate decreases with increasing density gradient.[49] Similar stabilization of tearing mode in the presence of diamagnetic drift by density gradient is observed in Ref. 2 when there is no temperature gradient present.

H. Effect of ion temperature gradient

The effect of ion dynamics on microtearing mode is inconclusive. The theoretical treatment of collisionless and semicollisional microtearing mode is without the ion dynamics, as $\triangle < \rho_i$ is considered, and ions are treated unmagnetized. On the other hand, for collisional case, $\triangle > \rho_i$ and ions enter the $\tilde{\phi}$ equation through polarization and FLR modification to $E \times B$ terms.[2] Even in the limit of $\triangle < \rho_i$, ion dynamics can play an important role in the stability properties of the microtearing mode through FLR stabilization effect.[41] However, ion dynamics has been observed to incur only limited effect on the microtearing mode[17,18,23–25,27] in gyrokinetic simulations. We consider ions to be always gyrokinetic in our simulations. Here, we do a $k_\theta \rho_s$ scan for real frequency and growth rate with and without the ion temperature gradient and plot in Fig. 9 for the finite collisional case. The ion temperature gradient lowers the real frequency of the microtearing mode and also stabilizes the mode partially. The effect of stabilization is more prominent at higher $k_\theta \rho_s$. With the removal of the ion temperature gradient, we are shutting off any free energy flow through ion channel, for example, the ITG/KBM mode, and therefore, the overall growth rate of the microtearing mode increases. The behavior remains the same even for the microtearing mode with $\nu_e = 0.0$.

I. Effect of impurity

In the present section, we remove the Carbon impurity and compare the results with those including Carbon impurity for $\nu_e = 5.577$. We do not set $Z_{eff} = 1$; therefore, the effective collision frequency, which depends on Z_{eff}, remains the same. In contrast to the effect of ion temperature gradient, the impurity, in this case, is found to be destabilizing as shown in Fig. 10. The impurity also increases the real frequency of the mode slightly. Similar observations are reported for microtearing mode in Ref. 24. We see it as thermal dilution of the ions by impurity ions, which can weaken the ion temperature gradient drive. This is in conformity with what has been observed in Section III H. When we set ion temperature gradient drive zero, the microtearing mode is destabilized. Similarly, when we introduce impurity, it weakens the ion temperature gradient drive, and therefore, the microtearing mode is destabilized further.

J. Role of electrostatic potential $\tilde{\phi}$

The effect of the electrostatic potential $\tilde{\phi}$ on microtearing mode is intriguing as there are no definitive conclusions regarding the role of $\tilde{\phi}$ in the stability properties of the mode. For example, $\tilde{\phi}$ is shown to have stabilizing effect on the collisionless case.[50] It is assumed to have no effect for the collisionless and semicollisional cases while shown to be stabilizing in the collisional case.[2] On the contrary, including

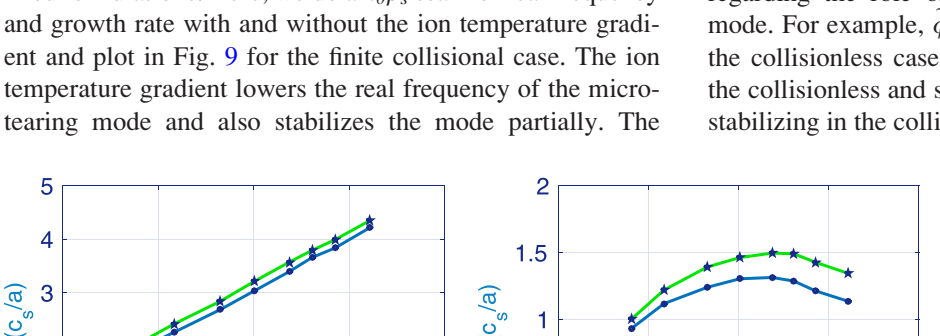

FIG. 10. Real frequency (left) and growth rate (right) vs $k_\theta \rho_s$ at $r/a = 0.93$, with and without Carbon impurity.

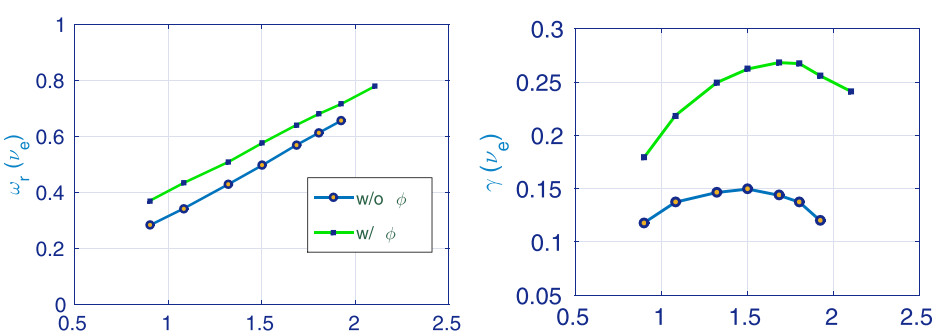

FIG. 11. Real frequency (left) and growth rate (right) vs $k_\theta\rho_s$ at $r/a = 0.93$, with and without the electrostatic potential $\tilde{\phi}$.

$\tilde{\phi}$ in the semi-collisional case is shown to be destabilizing.[3] In gyrokinetic simulations of toroidal systems, $\tilde{\phi}$ is observed to be ineffective on the top of the pedestal,[17] strongly destabilizing at the core,[18,37] destabilizing for lower q, but stabilizing at higher q.[28,29] In Fig. 11, we have shown the real frequency and growth rate for the finite collisional case with and without the electrostatic potential. The real frequency with $\tilde{\phi}$ is higher than that without $\tilde{\phi}$, and both increase linearly. The non-monotonic behavior of growth rate remains the same in both cases. However, the growth rate is substantially reduced with $\tilde{\phi} = 0$. The present parameters fall in the semi-collisional regime of Ref. 2, where the effect of $\tilde{\phi}$ is neglected. However, here, we observe substantial destabilization of the mode by including $\tilde{\phi}$. It is in conformity with the conclusion of the numerical solution[3] of the complete eigenmode equation of Ref. 2, where $\tilde{\phi}$ is found to be destabilizing. An explanation of the destabilization by $\tilde{\phi}$, from Ref. 3, can be given as follows: the electron heating rate is given by the quantity $\tilde{j}_\parallel \tilde{E}_\parallel$. In the presence of $\tilde{\phi}$, the value of $\tilde{E}_\parallel$ is reduced as $\tilde{E}_\parallel = -\nabla_\parallel \tilde{\phi} - \partial \tilde{A}_\parallel/\partial t$. Therefore, the electron heating is reduced, which means electrons draw less energy from the wave in the presence of $\tilde{\phi}$, and therefore, the mode is further destabilized when $\tilde{\phi}$ is present. However, we would like to mention here that such a speculation is based on what is observed in earlier slab calculations as in Ref. 3 and may not be the sole reason for destabilization by $\tilde{\phi}$ in the case of toroidal devices where the magnetic drifts and trapped particles have strong impact on the mode.[17,18] We observe similar destabilizing effect of $\tilde{\phi}$ also on the microtearing mode with $\nu_e = 0$.

K. Dependence on safety factor *q* and shear

In this section, we carry out safety factor q and shear scan and calculate the growth rates for the mode $k_\theta\rho_s \simeq 1.5$ with $\nu_e = 5.577$. These are plotted in Fig. 12. The left figure is for q scan with and without the presence of electrostatic potential. The growth rate increases with q and attains a maximum at around $q = 7$, and then the trend is reversed, and the growth rate starts decreasing with q. The case without $\tilde{\phi}$ behaves in a similar way; however, the peak is shifted towards lower q below $q = 6$. Over larger part of q, potential $\tilde{\phi}$ is destabilizing, but at very low q, the electrostatic potential turns out to be stabilizing. This is opposite to what is observed in Refs. 28 and 29. We see similar trend for the microtearing mode with zero collision frequency. The figure on the right shows the variation of the growth rate with shear $\hat{s}$. Similar to q scan, the growth rate increases, peaks, and then falls off with increasing shear. The case without $\tilde{\phi}$ follows similar trend. The non-monotonic behavior of the growth rate with respect to q and $\hat{s}$ can be explained[3] in terms of the ratio $L_n/L_s = Ln(\hat{s}/Rq)$, where $L_s = Rq/\hat{s}$ is the shear length. It has been observed in Ref. 3, including $\tilde{\phi}$ and non-constant ψ, that the growth rate of the microtearing mode increases with L_n/L_s, reaches a maximum, and then starts decreasing with further increase in L_n/L_s. For a given L_n, increasing $1/L_s = \hat{s}/Rq$, that is, increasing $\hat{s}$ or decreasing q can decrease the field line bending across the current layer,[3] where otherwise $\tilde{A}_\parallel$ can have sharp scales. Decreasing field line bending destabilizes the mode. However, a point is reached when the variations in $\tilde{A}_\parallel$ is reduced to such a level that it can be treated as constant over the current layer. When this constant ψ condition is attained, the growth rate decreases with $1/Ls$, that is increasing $\hat{s}$ or decreasing q.[3] However, it is to be noted that this explanation is based upon simple slab calculations where the magnetic drift effects are missing. The magnetic drift effects actually play a more important role than the simple slab drives in a toroidal geometry, as discussed in Refs. 17 and 18. In a

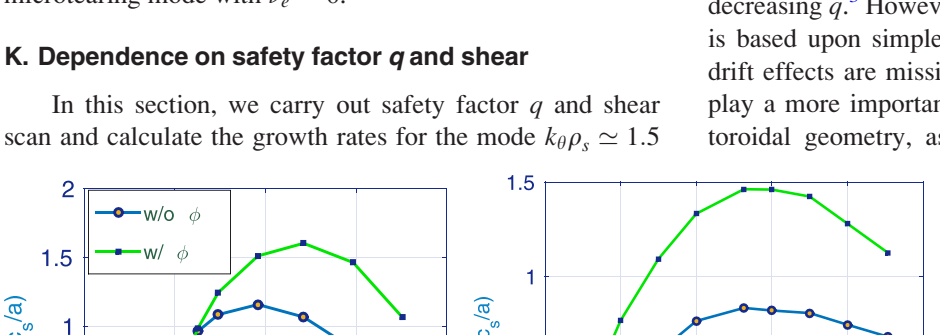

FIG. 12. Growth rate vs q (left) and shear $\hat{s}$ (right) at $k_\theta\rho_s = 1.5$, with and without electrostatic potential $\tilde{\phi}$.

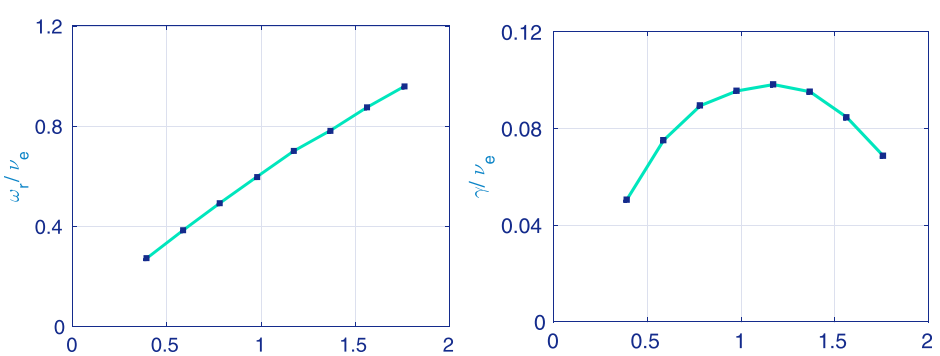

FIG. 13. Real frequency (left) and growth rate (right) with respect to $k_\theta\rho_s$.

toroidal geometry, the bounce frequency of trapped particles and the transit frequency of passing particles are proportional to the inverse of safety factor q. Therefore, changing q can change these frequencies. Also, it is shown in Ref. 17 that the shear affects the magnetic drift frequencies. Therefore, changing shear can change the magnetic drift frequency and hence alters the resonance between the mode frequency and the magnetic drift frequency. The behavior of the microtearing mode with respect to shear is what makes it distinguishable from other modes. The universal mode[51–54] is strongly stabilized by shear. The shear plays a stabilizing role also on drift modes.[55] Therefore, tweaking shear could be a reliable method to identify the microtearing mode[3,24] from other modes in tokamaks having real frequency rotating in the electron diamagnetic direction such as ETG, TEM,[56–58] etc. For example, for drift modes, the growth rates increase with decreasing shear. In contrast, the growth rate of the microtearing mode decreases as the shear decreases for low shear as shown in Fig. 12(b). Apart from experimental techniques such as velocimetry and Doppler backscattering with cross-polarization scattering, used in experiments[35,39] to identify the microtearing mode experimentally, methods to change the magnetic shear could be another way to corroborate the observation of the microtearing mode. In the low shear regime, with decreasing shear, the mode should become stronger if it is another drift mode and weaker if it is a microtearing mode. A shear profile is determined by a q profile. Methods of obtaining different q profiles by changing current profiles by using additional set of NBI injectors at different tangency radii are elaborately discussed in Ref. 59.

Note that the observed properties of the microtearing mode in the present case are in conformity with those observed in Ref. 17 for the edge in MAST. In our study, we have observed nonmonotonic dependence of the growth rates on the electron temperature gradient and electron β. The mode growth rate behaves nonmonotonically with respect to q and shear. Interestingly, the growth rates are observed to be independent of the collision frequency in the edge. These findings are qualitatively similar to those observed in the edge of MAST[17] where the magnetic drifts are found to be more important than the collisions for spherical tokamaks. The diversion of the mode properties from those predicted in earlier theories[2,3] based on slab models can be attributed to the presence of magnetic drift and trapped particles in spherical tokamaks[17,18] and other toroidal devices.[32–34,37,38]

IV. MICROTEARING MODE IN THE CORE OF NSTX

Next, we carry out a numerical study of the microtearing mode in the core of NSTX for a different set of parameters taken from Ref. 24. These parameters correspond to an NSTX discharge 120968. An elaborate description of the discharge can be found in Refs. 23 and 24. The local parameters at r/a $=0.6$ are as follows: $R/a = 1.52$, $\kappa = 1.71$, $\delta = 0.125$, $q_0 = 1.688$, $\hat{s} = 1.73$, $T_e/T_i = 0.967, T_c/T_i = 1.0, \rho^* = 0.0139$, $\nu_e(c_s/a) = 1.53$, $\beta_e = 0.0848$, $n_e(10^{19}\mathrm{m}^{-3}) = 6.0, T_e(\mathrm{keV}) = 0.45$, $R/L_{Ti} = 3.587, R/L_{Te} = 4.134, R/L_{Tc} = 3.587, R/L_{ne} = -1.262$, $R/L_{nc} = -4.18$, Carbon impurity concentration $n_c/n_e = 0.064$, $Z_{eff} = 2.9$, and no E_r shear. For the present analysis, we consider the following numerical parameters: time step $\triangle t c_s/a \approx 0.0017$, spatial grid size $\triangle x \approx 0.0092\rho_s$ $\triangle y \approx 0.2\rho_s$, and particle per species ≈ 2 million. In the following, we present linear results on the microtearing mode in the core to find out the dependence of the mode on various plasma parameters. We then compare and contrast these results with those for the edge microtearing mode discussed in Section III.

A. $k_\theta\rho_s$ scan

The real frequency and growth rate are calculated varying toroidal mode number n and shown in Fig. 13 normalized by the experimental value of the collision frequency as a function of $k_\theta\rho_s$. The real frequency in the left panel increases linearly with $k_\theta\rho_s$ because it is a function of the diamagnetic drift frequency which, in turn, is a function of $k_\theta\rho_s$. Therefore, the mode exhibits the drift-mode characteristics. The growth rate increases initially and then decreases at higher $k_\theta\rho_s$. The reason for such a behavior is elucidated in the previous Section III C. There are, however, two main differences between the microtearing mode in the edge and core: 1. the growth rate for the edge case peaks at higher $k_\theta\rho_s$ and has a broader k spectrum, while the mode at the core peaks at relatively lower $k_\theta\rho_s$ and, therefore, has narrower $k_\theta\rho_s$ spectrum, and 2. the real frequency when normalized to the collision frequency has the same range, that is, $\omega_r/\nu_e \leq 1.0$, while the growth rate normalized by ν_e is much lower in the core than that in the edge. The mode structures for $\tilde{A}_\parallel$ and $\tilde{\phi}$ are observed to have even and odd parities, respectively, as expected for a microtearing mode (not shown).

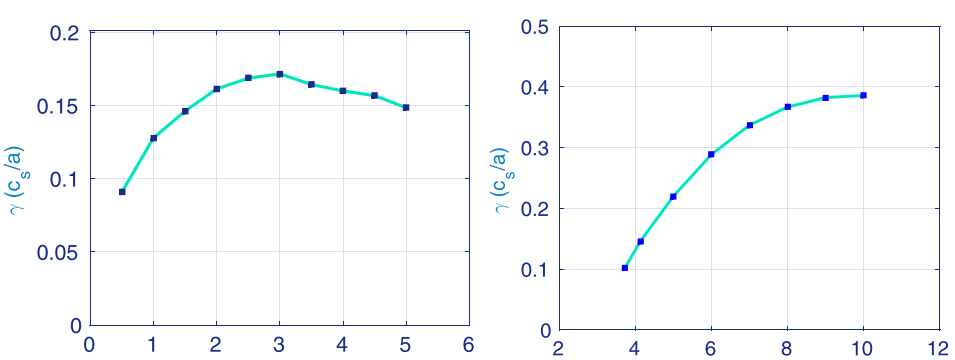

FIG. 14. Growth rates with respect to variations in $e-i$ collision frequency (left) and electron temperature gradient (right) for $k_\theta \rho_s \simeq 1.0$.

B. Dependence on collision frequency and ∇T_e

Next, we check for the dependency on collisions. The left panel of Fig. 14 presents the dependence of the microtearing mode growth rate on collision frequency. The growth rate increases with collision frequency, attains a maximum, and then decays with increasing collision frequency. This is in sharp contrast with what have been observed in the edge case, where the growth rate appears to be virtually independent of the collision frequency over a large range. However, the present observation conforms to the conventional wisdom vis-a-vis microtearing mode.[3] The growth rate increases with ν_e initially because it is the collisions that allow to "tap the free energy"[4] available in ∇T_e. This behavior of the growth rate with respect to the collision frequency is also in conformity with that of Ref. 24. The reason for non-monotonic nature of the dependence of growth rate on collisions is that at very high collisions, the electron motion becomes so diffusive ($\Omega_{Doppler} \propto 1/\nu_e$) that it becomes difficult for the electrons to form and maintain a perturbed current layer[17,28,29] hindering the sustenance of the microtearing mode. We also change the electron temperature gradient and calculate the corresponding growth rates of the mode to show the source of free energy. It is plotted in the right panel of Fig. 14. The growth rate increases initially with R/L_{Te} indicating that ∇T_e is the main source of the drive. There is a threshold in the R/L_{Te} above which the mode comes into existence. The quantity $\triangle'$ is negative for high n modes, and the tearing modes are stabilized at higher n in the absence of temperature gradient. A minimum of ∇T_e is, therefore, required to overcome the stabilization effect of negative $\triangle'$. At very high R/L_{Te}, the growth rate tends to saturate. If the value of R/L_{Te} is further increased, the growth rate starts decaying. It is similar to the observation in the case of microtearing mode in the edge discussed in Sec. III, and the same explanation applies also in this case.

C. Dependence on β

The other important parameter for the microtearing mode is β_e. We show the dependence of the growth rate and real frequency on β_e in Fig. 15. The real frequency decreases with increasing β_e. The growth rate, on the other hand, increases with β_e. However, similar to the edge mode in Sec. III, the dependence of growth rates on β_e is non-monotonic. At very high value of β_e, the growth rate starts saturating and eventually decreases with increasing β_e. As explained in the edge case, this is related to the increased magnetic field line bending to overcome the destabilizing drive of the electron temperature gradient.

D. Effect of electrostatic potential $\tilde{\phi}$

Next, we study the effect of $\tilde{\phi}$ on the microtearing mode in the core. In Fig. 16, the real frequency and growth rate are shown as a function of $k_\theta \rho_s$ with and without $\tilde{\phi}$. The real frequency with $\tilde{\phi}$ is higher than that without $\tilde{\phi}$. However, the growth rate is found to get enhanced when $\tilde{\phi}$ is removed. Thus, in contrast to the microtearing mode in the edge discussed in Section III J, the electrostatic potential $\tilde{\phi}$ here plays a stabilizing role. Intuitively, such a role of $\tilde{\phi}$ is observed in the collisional case[2] where the current layer width is determined by the condition $\tilde{E}_\parallel = 0$ rather than $\omega = \Omega_{Doppler} = k_\parallel^2 v_\parallel^2/\nu_e$ and $\tilde{E}_\parallel = 0$ is obtained when $\tilde{\phi}$ component in $\tilde{E}_\parallel$ shorts out the inductive component. Thus, $\tilde{\phi}$ in the collisional regime can stabilize the mode. We note from Fig. 16 that although ω is only slightly less than ν_e, the growth rate γ, on the other hand, is much less than the

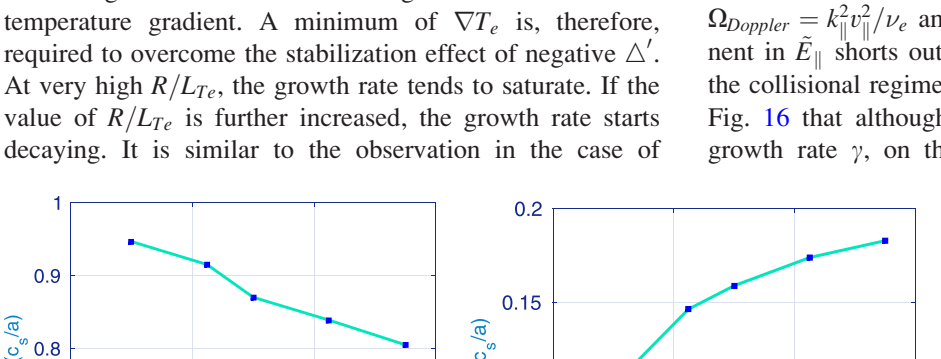

FIG. 15. Real frequency (left) and growth rate (right) with respect to electron β_e for $k_\theta \rho_s \simeq 1.0$.

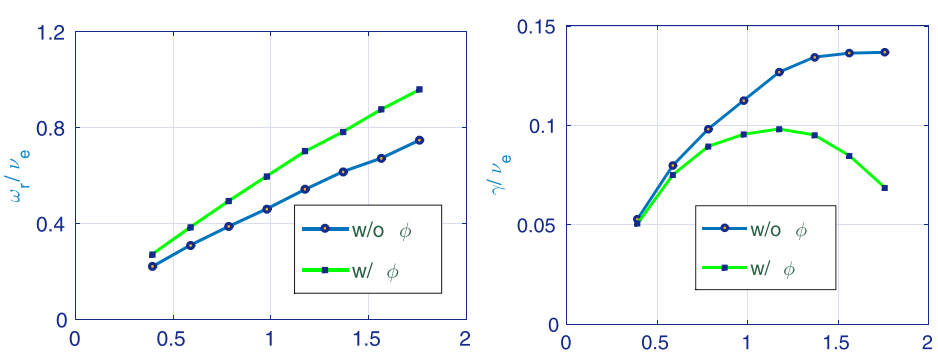

FIG. 16. Real frequency (left) and growth rate (right) versus $k_\theta\rho_s$ with and without $\tilde{\phi}$.

collision frequency ν_e which should satisfy the collisional condition for tearing mode (zero real frequency). But, when we put the values of the parameters in Eqs. (1) and (2), the parameters actually satisfy the condition for the semi-collisional rather than the collisional regime.

It is worth mentioning here that the electrostatic potential is found to be destabilizing in the core of MAST.[18] Although a clear explanation is not available, this type of discrepancy can be attributed to the presence of complex physics of present day tokamaks[17,18,37] in contrast to the theories with simpler assumptions. In particular, for spherical tokamaks, the magnetic drifts have a very important effect in making the microtearing modes unstable as observed in Refs. 17 and 18. This drive mechanism could not be captured in earlier slab theories.[2,3]

We also carry out q and shear $\hat{s}$ scans. Increasing q is found to be stabilizing, while $\hat{s}$ behaves non-monotonically. The microtearing mode in the core also varies with density gradient. The growth rate decreases with increasing density gradient and holds finite growth rate even at $R/L_n = 0$. The impurity and ion temperature gradient have mild effect on the microtearing mode. These results are in conformity with those discussed in Ref. 24 and not shown here. The properties of the microtearing mode in the core are also observed to be in conformity with those reported in the core of MAST.[18] The mode growth rates are strongly dependent upon the collision frequency in the core. However, $\tilde{\phi}$ in the core of NSTX is found to be stabilizing, whereas it is destabilizing in the core of MAST.

V. MICROTEARING MODE IN CONVENTIONAL TOKAMAK

For the sake of completeness, we discuss the microtearing mode for the conventional tokamak parameters also. These parameters are taken from Ref. 30 and are relevant to "JET like" scenario but do not correspond to any specific JET plasma discharge. They are as follows: $r/a=0.6, R/a=3.3, \kappa=1.70, \delta=0.37, q_0=1.45$, $\hat{s}=1.32, T_e/T_i=1.0, T_c/T_i=1.0$, $\rho^*=0.005, \nu_e(c_s/a)=0.43, \beta_e=0.0380$, $n_e(10^{19}\mathrm{m}^{-3})=7.8, T_e(\mathrm{keV})=1.25$, $R/L_{Ti}=7.128, R/L_{Te}=7.128$, $R/L_{Tc}=7.128, R/L_{ne}=0.495, R/L_{nN}=0.462$, Nitrogen impurity concentration $n_N/ne=0.05$, $Z_{eff}=3.41$, and no E_r shear. We consider the following numerical parameters: time step $\triangle tc_s/a\approx 0.0025$, grid size $\triangle x\approx 0.013\rho_s$, $\triangle y\approx 0.215\rho_s$, and particle per species ≈ 2 million.

A. $k_\theta\rho_s$ scan

Firstly, we carry out a $k_\theta\rho_s$ scan for real frequency and growth rate (Fig. 17). The real frequency increases almost linearly. The growth rate, on the other hand, behaves non-monotonically as in the preceding cases. It increases with $k_\theta\rho_s$, peaks at around $k_\theta\rho_s = 0.8$, and then decays. The mode structures are even for $\tilde{A}_\parallel$ and odd for $\tilde{\phi}$ (not shown). For these parameters, the peak is at higher $k_\theta\rho_s$ as compared to that expected for a conventional tokamak.[28,29] A similar observation is reported in Ref. 30 also. The difference with the microtearing modes in the edge and core of NSTX discussed above is that $\omega > \nu_e$ here, while in the preceding cases, $\omega < \nu_e$ always. The growth rate in this case is less than the collision frequency ν_e. This is similar to the other two cases discussed above. When we fit the physical parameters to Eqs. (1) and (2), they satisfy the criteria for semi-collisional regime.

B. Electron temperature gradient and β_e scan

The growth rate as a function of electron temperature gradient R/L_{Te} is shown in the left panel of Fig. 18. It

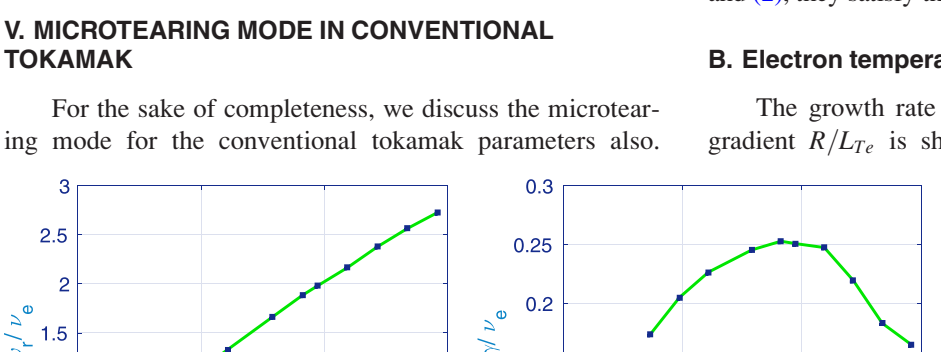

FIG. 17. Real frequency (left) and growth rate (right) versus $k_\theta\rho_s$.

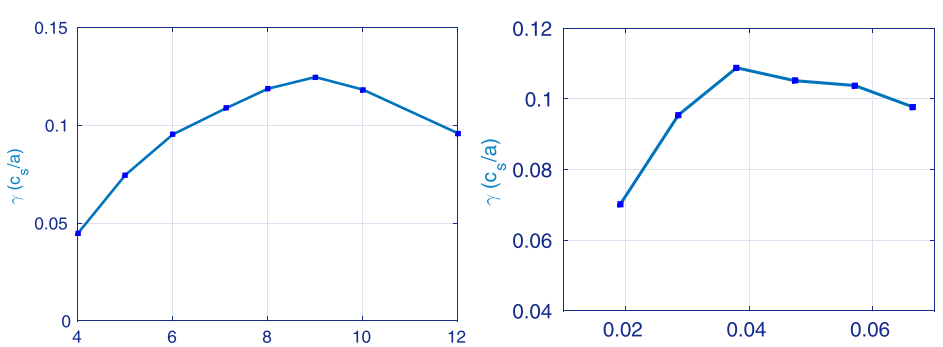

FIG. 18. Growth rates as a function of electron temperature gradient (left) and β_e (right) for $k_\theta \rho_s \simeq 0.9$.

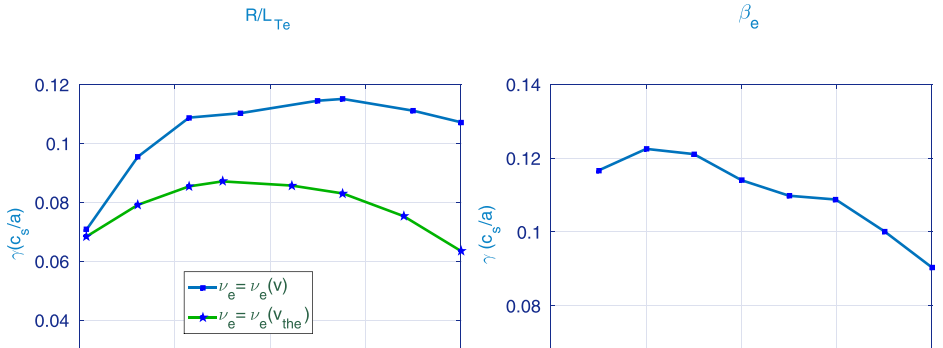

FIG. 19. Growth rates versus ν_e (left) and R/L_{ne} (right) for $k_\theta \rho_s \simeq 0.9$.

increases initially and then at higher value of R/L_{Te} starts falling. The growth rate versus β_e is displayed in the right panel. The growth rate increases with β_e, peaks around $\beta_e \simeq 0.04$, and then rolls off. Both these properties have been observed in earlier two cases and can be explained by the same physics and are inherent characters of the microtearing mode.

C. Collision frequency and R/L_{ne} scan

The dependence of the mode on collision frequency is shown in the left panel of Fig. 19 for $k_\theta \rho_s \simeq 0.9$. Two cases have been shown: one having velocity dependent collision frequency and the other with velocity independent collision frequency. In the latter case, $\nu_e(v)$ is converted to $\nu_e(v_{the})$, where v_{the} is the electron thermal velocity, following Ref. 18. The growth rate increases with ν_e in both cases. At very high value, however, growth rate slowly starts decreasing. Testing the velocity dependence of collisions is motivated by earlier analytical theories, which predict that a velocity-dependent collision frequency is necessary for instability.[1,2,5] In contrast to these analytical predictions, here we observe that the velocity dependence in the collision frequency is not a strict requirement for the microtearing mode in a toroidal device, where the magnetic drift resonance, trapped particles, finite orbit width of the particles, etc., can play a more critical role than the velocity dependence of collision frequency in the stability properties of the mode.[18,25,38] The right panel of Fig. 19 shows the growth rate versus density gradient. The growth rate decreases with increasing density gradient and exhibits finite growth rate even when density gradient is zero or negative.

D. Role of electrostatic potential

We also study the effect of the electrostatic potential $\tilde{\phi}$ on the core microtearing mode for the conventional tokamak parameters considered in this section. The real frequency and growth rate are shown in Fig. 20. The real frequency including $\tilde{\phi}$ is slightly higher than that without $\tilde{\phi}$. The growth rate, on the other hand, increases when $\tilde{\phi}$ is included. This core result is opposite to what is observed in the core case for NSTX in Sec. II above, where $\tilde{\phi}$ is found to be stabilizing. It is instead similar to what we observe in the edge of

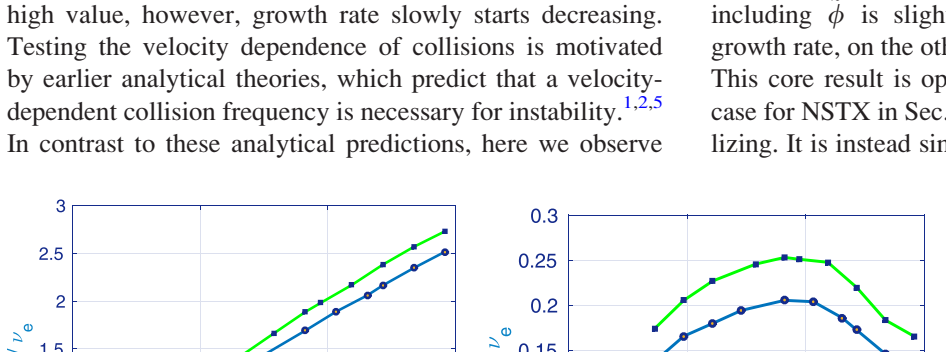

FIG. 20. Real frequency (left) and growth rate (right) with respect to $k_\theta \rho_s$ with and without $\tilde{\phi}$.

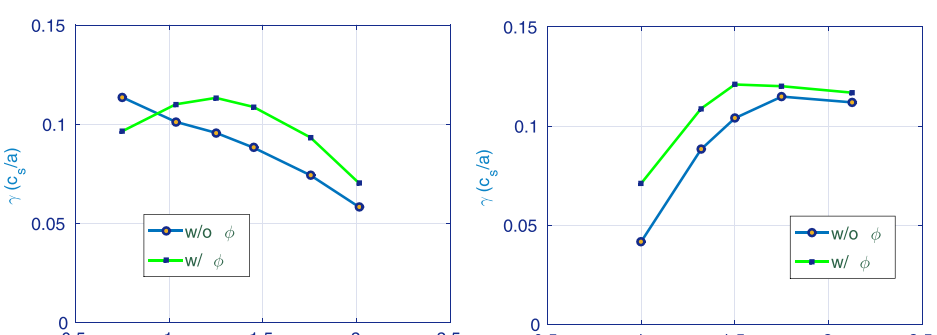

FIG. 21. Growth rates versus q and shear $\hat{s}$ with and without $\tilde{\phi}$ for $k_\theta \rho_s \simeq 0.9$.

NSTX. When we evaluate the conditions in Eqs. (1) and (2), it appears that the present parameters fall in the semi-collisional category. Therefore, the destabilization can be understood in the same way as in the edge of NSTX.

E. Effect of *q* and shear $\hat{s}$

We plot growth rate against q and $\hat{s}$ with and without $\tilde{\phi}$ in Fig. 21 for the mode corresponding to $k_\theta \rho_s \simeq 0.9$. The growth rate increases with increasing q and then decays at higher values. The growth rate without $\tilde{\phi}$, however, decreases monotonically with q. The electrostatic potential $\tilde{\phi}$ is found to be stabilizing at very low q as observed in the case of the edge microtearing mode. The growth rate versus shear $\hat{s}$ increases initially and tends to decrease slowly at higher values of $\hat{s}$. The case without $\tilde{\phi}$ follows similar trend.

VI. SUMMARY

In this paper, we present a detailed linear study of the microtearing mode in the edge as well as core of NSTX. Some interesting characters of the microtearing mode are observed. Although the microtearing modes exhibit similar behavior with respect to the dependence on β_e and electron temperature gradient, we observe notable difference in the dependence of the mode on collisions and effect of $\tilde{\phi}$ on the instability in the edge and core. We find that the edge microtearing mode is virtually independent of collisions over a wide range of values, with no minimum threshold for collision frequency. These edge microtearing modes exist even when the collision frequency is zero. This might particularly be important for the future tokamaks which will be operating at further higher temperatures where collision frequency is very small. The microtearing mode in the core, on the other hand, exhibits non-monotonic dependence on the collision frequency and is unstable beyond a certain critical value of ν_e and stable at very high collision frequency. The edge microtearing mode peaks at higher $k_\theta \rho_s$ and has a broader spectrum. The electrostatic potential is destabilizing in the case of edge microtearing mode while stabilizing in the core of NSTX. Although electron temperature gradient and β_e thresholds are needed for the microtearing modes, we observe stabilization at higher values of R/L_{Te} and β_e. These results are then compared to those from the core of a conventional tokamak. The behavior of the latter microtearing mode remains the same with respect to R/L_{Te}, β_e, and ν_e when compared to the core microtearing mode in NSTX. However, the electrostatic potential $\tilde{\phi}$ affects the mode in a similar way as the edge microtearing mode of NSTX. We also tested the effect of the velocity dependence of collision frequency. In tokamak, it does not appear to be essential for the mode instability as also reported in Ref. 18.

Note that the observed properties of the microtearing mode in the edge are quite similar to those observed in Ref. 17 for MAST, where the growth rates are found to be independent of the collision frequency and are strongly dependent upon the magnetic drift resonance, supported by the nonmonotonic dependence of the growth rate and real frequency with respect to the electron temperature gradient. The properties of the microtearing mode in the core, similarly, are found to be in conformity with those reported in the core of MAST.[18] The mode in the core is strongly dependent upon the collision frequency. However, $\tilde{\phi}$ in the core of NSTX is found to be stabilizing, whereas it is destabilizing in the core of MAST. This difference is a subject of further investigation. The observed discrepancy of the mode properties with those predicted in the earlier theories can be attributed to the presence of complex physics such as magnetic drifts and trapped particles, etc., in the toroidal devices.[17,18,32–34,37,38]

ACKNOWLEDGMENTS

This material is based upon work supported in part by the U.S. Department of Energy under Award No. DE-FG02-08ER54954 and is also part of the DOE Scientific Discovery Through Advanced Computing (SciDAC) Edge Physics Simulation (EPSI) project. It uses the resources of the National Energy Research Scientific Computing Center (NERSC), a DOE Office of Science user facility. We thank D. Ernst, MIT for useful discussion.

[1]R. D. Hazeltine, D. Dobrott, and T. S. Wang, Phys. Fluids **18**, 1778 (1975).
[2]J. F. Drake and Y. C. Lee, Phys. Fluids **20**, 1341 (1977).
[3]N. T. Gladd, J. F. Drake, C. L. Chang, and C. S. Liu, Phys. Fluids **23**, 1182 (1980).
[4]D. A. D'Ippolito, Y. C. Lee, and J. F. Drake, Phys. Fluids **23**, 771 (1980).
[5]A. B. Hassam, Phys. Fluids **23**, 38 (1980).
[6]A. B. Hassam, Phys. Fluids **23**, 2493 (1980).
[7]J. W. Connor, S. C. Cowley, and R. J. Hasti, Plasma Phys. Controlled Fusion **32**, 799 (1990).
[8]P. J. Catto and M. N. Rosenbluth, Phys. Fluids **24**, 243 (1981).
[9]X. Garbet, F. Mourgues, and A. Samain, Plasma Phys. Controlled Fusion **30**, 343 (1988).
[10]X. Garbet, F. Mourgues, and A. Samain, Plasma Phys. Controlled Fusion **32**, 131 (1990).

[11]J. F. Drake, N. T. Gladd, C. S. Liu, and C. L. Chang, Phys. Rev. Lett. **44**, 994 (1980).
[12]H. P. Furth, P. H. Rutherford, and H. Selberg, Phys. Fluids **16**, 1054 (1973).
[13]A. H. Glasser, J. M. Green, and J. L. Johnson, Phys. Fluids **18**, 875 (1975).
[14]J. F. Drake and Y. C. Lee, Phys. Rev. Lett. **39**, 453 (1977).
[15]J. M. Canik, W. Guttenfelder, R. Maingi, T. H. Osborne, S. Kubota, Y. Ren, R. E. Bell, H. W. Kugel, B. P. LeBlanc, and V. A. Souhkanovskii, Nucl. Fusion **53**, 113016 (2013).
[16]D. Dickinson, C. M. Roach, S. Saarelma, R. Scannell, A. Kirk, and H. R. Wilson, Phys. Rev. Lett. **108**, 135002 (2012).
[17]D. Dickinson, C. M. Roach, S. Saarelma, R. Scannell, A. Kirk, and H. R. Wilson, Plasma Phys. Controlled Fusion **55**, 074006 (2013).
[18]D. J. Applegate, C. M. Roach, J. W. Connor, S. C. Cowley, W. Dorland, R. J. Hastie, and N. Joiner, Plasma Phys. Controlled Fusion **49**, 1113 (2007).
[19]D. J. Applegate, C. M. Roach, S. C. Cowley, W. D. Dorland, N. Joiner, R. J. Akers, N. J. Conway, A. R. Field, A. Patel, M. Valovic, and M. J. Walsh, Phys. Plasmas **11**, 5085 (2004).
[20]K. L. Wong, S. Kaye, D. R. Mikkelsen, J. A. Krommes, K. Hill, R. Bell, and B. LeBlanc, Phys. Rev. Lett. **99**, 135003 (2007).
[21]D. R. Smith, W. Guttenfelder, B. P. LeBlanc, and D. R. Mikkelsen, Plasma Phys. Controlled Fusion **53**, 035013 (2011).
[22]W. Guttenfelder, J. Candy, S. M. Kaye, W. M. Nevins, E. Wang, R. E. Bell, G. W. Hammett, B. P. LeBlanc, D. R. Mikkelsen, and H. Yuh, Phys. Rev. Lett. **106**, 155004 (2011).
[23]W. Guttenfelder, J. Candy, S. M. Kaye, W. M. Nevins, E. Wang, J. Zhang, R. E. Bell, N. A. Crocker, G. W. Hammett, B. P. LeBlanc, D. R. Mikkelsen, Y. Ren, and H. Yuh, Phys. Plasmas **19**, 056119 (2012).
[24]W. Guttenfelder, J. Candy, S. M. Kaye, W. M. Nevins, R. E. Bell, G. W. Hammett, B. P. LeBlanc, and H. Yuh, Phys. Plasmas **19**, 022506 (2012).
[25]C. M. Roach, D. J. Applegate, J. W. Connor, S. C. Cowley, W. D. Dorland, R. J. Hastie, N. Joiner, S. Saarelma, A. A. Schekochihin, R. J. Akers, C. Brickley, A. R. Field, M. Valovic, and MAST Team, Plasma Phys. Controlled Fusion **47**, B323 (2005).
[26]J. Kesner and S. Migliuolo, Nucl. Fusion **39**, 163 (1999).
[27]D. Told, F. Jenko, P. Xanthopoulos, L. D. Horton, E. Wolfrum, and ASDEX Upgrade Team, Phys. Plasmas **15**, 102306 (2008).
[28]H. Doerk, F. Jenko, M. J. Pueschel, and D. R. Hatch, Phys. Rev. Lett. **106**, 155003 (2011).
[29]H. Doerk, F. Jenko, T. Görler, D. Told, M. J. Pueschel, and D. R. Hatch, Phys. Plasmas **19**, 055907 (2012).
[30]S. Moradi, I. Pusztai, W. Guttenfelder, T. Fülöp, and A. Mollen, Nucl. Fusion **53**, 063025 (2013).
[31]S. Saarelma, M. N. A. Beurskens, D. Dickinson, L. Frassinetti, M. J. Leyland, C. M. Roach, and EFDA-JET Contributors, Nucl. Fusion **53**, 123012 (2013).
[32]A. K. Swamy, R. Ganesh, J. Chowdhury, S. Brunner, J. Vaclavik, and L. Villard, Phys. Plasmas **21**, 082513 (2014).
[33]A. K. Swamy, R. Ganesh, J. Chowdhury, S. Brunner, J. Vaclavik, and L. Villard, J. Phys., Conf. Ser. **561**, 012017 (2014).
[34]A. K. Swamy, R. Ganesh, S. Brunner, J. Vaclavik, and L. Villard, Phys. Plasmas **22**, 072512 (2015).
[35]P. Manz, J. E. Boom, E. Wolfrum, G. Birkenmeier, I. G. J. Classen, N. C. Luhmann, Jr., U. Stroth, and ASDEX Upgrade Team, Plasma Phys. Controlled Fusion **56**, 035010 (2014).
[36]Y. Hamada, T. Watari, A. Nishizawa, O. Yamagishi, K. Narihara, K. Ida, Y. Kawasumi, T. Ido, M. Kojima, K. Toi, and JIPPT-IIU Group, Nucl. Fusion **55**, 043008 (2015).
[37]I. Predebon, F. Sattin, M. Veranda, D. Bonfiglio, and S. Cappello, Phys. Rev. Lett. **105**, 195001 (2010).
[38]I. Predebon and F. Sattin, Phys. Plasmas **20**, 040701 (2013).
[39]J. C. Hillesheim, D. Dickinson, C. M. Roach, S. Saarelma, R. Scannell, A. Kirk, N. A. Crocker, W. A. Peebles, H. Meyer, and MAST Team, Plasma Phys. Controlled Fusion **58**, 014020 (2016).
[40]D. R. Hatch, M. J. Pueschel, F. Jenko, W. M. Nevins, P. W. Terry, and H. Doerk, Phys. Plasmas **20**, 012307 (2013).
[41]S. C. Cowley, R. M. Kulsrud, and T. S. Hahm, Phys. Fluids **29**, 3230 (1986).
[42]Y. Chen and S. E. Parker, J. Comput. Phys. **189**, 463 (2003).
[43]Y. Chen and S. E. Parker, J. Comput. Phys. **220**, 839 (2007).
[44]W. Wan, Y. Chen, and S. Parker, Phys. Plasmas **12**, 012311 (2005).
[45]Y. Chen, J. Chowdhury, S. E. Parker, and W. Wan, Phys. Plasmas **22**, 042111 (2015).
[46]Y. Chen, J. Chowdhury, N. Maksimovic, S. E. Parker, and W. Wan, "Gyro-kinetic Ion drift-kinetic electron simulation of the cylindrical (m = 2, n = 1) tearing mode," Phys. Plasmas (to be published).
[47]W. W. Lee, J. Comput. Phys. **72**, 243 (1987).
[48]W. Wan, S. E. Parker, Y. Chen, Z. Yan, R. J. Groebner, and P. B. Snyder, Phys. Rev. Lett. **109**, 185004 (2012).
[49]J. Weiland, *Collective Modes in Inhomogeneous Plasma* (IOP Publishing Ltd., 2000).
[50]B. Coppi, J. W. K. Mark, L. Sugiyama, and G. Bertin, Phys. Rev. Lett. **42**, 1058 (1979).
[51]D. W. Ross and S. M. Mahajan, Phys. Rev. Lett. **40**, 324 (1978).
[52]K. T. Tsang, P. J. Catto, J. C. Whitson, and J. Smith, Phys. Rev. Lett. **40**, 327 (1978).
[53]J. Chowdhury, R. Ganesh, S. Brunner, J. Vaclavik, and L. Villard, Phys. Plasmas **17**, 102105 (2010).
[54]M. Landreman, T. M. Antonsen, Jr., and W. Dorland, Phys. Rev. Lett. **114**, 095003 (2015).
[55]W. Horton, Rev. Mod. Phys. **71**, 735 (1999).
[56]F. Jenko, W. Dorland, M. Kotschenreuther, and B. N. Rogers, Phys. Plasmas **7**, 1904 (2000).
[57]J. Lang, Y. Chen, and S. E. Parker, Phys. Plasmas **14**, 082315 (2007).
[58]J. Lang, S. E. Parker, and Y. Chen, Phys. Plasmas **15**, 055907 (2008).
[59]S. P. Gerhardt, R. Andre, and J. E. Menard, Nucl. Fusion **52**, 083020 (2012).